AGU PUBLICATIONS

Geophysical Research Letters

RESEARCH LETTER
10.1002/2017GL076282

Key Points:
- First report of high and middle latitude neutral mesospheric density response to geomagnetic storms
- Statistical analysis indicates that mesospheric density under the auroral zone has a more than ~10% decrease in response to storms
- The decrease to mesospheric density due to intense geomagnetic storms extends to middle latitudes

Supporting Information:
- Supporting Information S1
- Table S1

Correspondence to:
I. M. Reid and X. Xue,
iain.reid@adelaide.edu.au;
xuexh@ustc.edu.cn

Citation:
Yi, W., Reid, I. M., Xue, X., Murphy, D. J., Hall, C. M., Tsutsumi, M., … Dou, X. (2018). High- and middle-latitude neutral mesospheric density response to geomagnetic storms. *Geophysical Research Letters*, *45*, 436–444. https://doi.org/10.1002/2017GL076282

Received 3 NOV 2017
Accepted 27 DEC 2017
Accepted article online 3 JAN 2018
Published online 12 JAN 2018

High- and Middle-Latitude Neutral Mesospheric Density Response to Geomagnetic Storms

Wen Yi[1,2,3], Iain M. Reid[3,4], Xianghui Xue[1,2,5], Damian J. Murphy[6], Chris M. Hall[7], Masaki Tsutsumi[8], Baiqi Ning[9], Guozhu Li[9], Joel P. Younger[3,4], Tingdi Chen[1,2], and Xiankang Dou[1]

[1]CAS Key Laboratory of Geospace Environment, Department of Geophysics and Planetary Sciences, University of Science and Technology of China, Hefei, China, [2]Mengcheng National Geophysical Observatory, School of Earth and Space Sciences, University of Science and Technology of China, Hefei, China, [3]School of Physical Sciences, University of Adelaide, Adelaide, South Australia, Australia, [4]ATRAD Pty Ltd., Thebarton, South Australia, Australia, [5]Synergetic Innovation Center of Quantum Information and Quantum Physics, University of Science and Technology of China, Hefei, China, [6]Australian Antarctic Division, Kingston, Tasmania, Australia, [7]Tromsø Geophysical Observatory, UiT-The Arctic University of Norway, Tromsø, Norway, [8]National Institute of Polar Research, Tachikawa, Japan, [9]Key Laboratory of Earth and Planetary Physics, Institute of Geology and Geophysics, Chinese Academy of Sciences, Beijing, China

Abstract We report the first observations of a high- and middle-latitude neutral mesospheric density response to geomagnetic storms. Interhemisphere mesospheric densities are estimated using data from meteor radars at Davis Station (68.6°S, 77.9°E), Svalbard (78.3°N, 16°E) and Tromsø (69.6°N, 19.2°E), which are located under the auroral zone; the Mohe (53.5°N, 122.3°E), and Beijing (40.3°N, 116.2°E) meteor radars, located in northern midlatitudes, and the Microwave Limb Sounder (MLS) on the Aura satellite. Both case studies and a superposed epoch analysis indicate that geomagnetic storms can significantly influence mesospheric density, causing a greater than ~10% decrease in the auroral zones and a ~5% decrease at higher midlatitudes. With such large changes, it is reasonable to suspect that geomagnetic storms influence the dynamics of the high and middle latitudes mesosphere.

1. Introduction

The mesosphere is dominated by dynamical influences from the lower atmosphere, including atmospheric tides, gravity waves, and planetary waves (e.g., Forbes & Garrett, 1979; Fritts & Alexander, 2003; Salby, 1984). The mesospheric variability produced by these waves has a clear seasonal and latitudinal dependence, with different characteristics in different seasons and latitudes. In addition to coupling from the lower atmosphere, the mesosphere is also influenced by geomagnetic effects produced by solar activity through the interaction between the solar wind and the Earth's magnetosphere-ionosphere-thermosphere (MIT) system. Many studies have reported that geomagnetic activity can significantly affect global mesospheric composition through energetic particle precipitation into the middle atmosphere. This leads to a large increase in odd nitrogen and odd hydrogen, and a strong depletion of ozone in the global mesosphere (e.g., Andersson, Verronen, Rodger, Clilverd, & Wang, 2014; Andersson, Verronen, Rodger, Clilverd, & Seppälä, 2014; Daae et al., 2012; Gao et al., 2017; Jackman et al., 2005; Solomon et al., 1983, and references therein). A few studies have found evidence for mesospheric temperature enhancements in polar and higher midlatitudes regions during geomagnetic storms (e.g., Hocke, 2017; von Savigny et al., 2007; Yuan et al., 2015). Recently, Yi, Reid, Xue, Younger, Spargo, et al. (2017) and Yi, Reid, Xue, Younger, Murphy, et al. (2017) reported that the southern polar mesosphere showed a clear response to recurrent geomagnetic activity in the declining phase of solar cycles 23 and 24.

The existing distribution of meteor radars, located from polar to midlatitude regions, permits an estimate of neutral mesosphere density and provides a favorable temporal and spatial coverage for examining the variability of mesospheric density from polar to midlatitudes during geomagnetic storms. In this paper, we report a statistical analysis of the global mesospheric density response to geomagnetic storms in solar cycles 23 and 24.

2. Data and Analysis

2.1. Estimation of Neutral Mesospheric Density

In this study, data from five meteor radars located at Davis Station (68.6°S, 77.9°E, magnetic latitude, 76°S), Svalbard (78.3°N, 16°E, magnetic latitude, 75°N), Tromsø (69.6°N, 19.2°E, magnetic latitude, 67.1°N), Mohe

(53.5°N, 122.3°E, magnetic latitude, 43.9°N), and Beijing (40.3°N, 116.2°E, magnetic latitude, 30.5°N) (hereinafter referred to DMR, SMR, TMR, MMR, and BMR, respectively) were used. These meteor radars all belong to the ATRAD meteor detection radar (MDR) series and are similar to the Buckland Park meteor radar system described by Holdsworth et al. (2004) and used in related studies (e.g., Hall et al., 2006; Liu et al., 2016; Yi, Reid, Xue, Younger, Spargo, et al., 2017). Table S1 (in the supporting information) summarizes the main system parameters, geographic and geomagnetic locations, and the observational time periods for these meteor radars.

The Microwave Limb Sounder (MLS) instrument is on board the Earth Observing System (EOS) Aura spacecraft, which was launched in 2004. Aura/MLS temperature (Schwartz et al., 2008) and geopotential height data (version 4) from August 2004 to December 2016 were restricted to data obtained within a 10° × 20° bounding box centered on these meteor radar locations. The daily averaged MLS temperature and geopotential height observations were interpolated into 1 km bins between 85 and 95 km, to produce temperature profiles using geometric heights obtained from geopotential heights (see, e.g., Younger et al., 2014; Yi, Reid, Xue, Younger, Murphy, et al., 2017).

The daily neutral mesospheric densities from 85 to 95 km were estimated using the daily ambipolar diffusion coefficients (D_a) from the five meteor radars and the MLS temperatures. The density retrieval approach (see, e.g., Takahashi et al., 2002; Yi, Reid, Xue, Younger, Murphy, et al., 2017) and the relative uncertainties in density are described in the Method section and Table S2 in the supporting information. The relative uncertainties in density were derived by using simultaneous meteor echoes observed by two colocated meteor radars with different frequencies (33 MHz and 55 MHz) at Davis Station (see Younger et al., 2014). A more detailed discussion of this intercomparison will be described in a forthcoming paper and include detailed density estimates and the associated error estimation in the derived densities.

The mesospheric densities estimated from the five meteor radars show different seasonal and latitudinal variations and that these results will also be described in subsequent work. In this study, we focus on the short-term variation of mesospheric density during geomagnetic storms, and so we remove variations with periods longer than 30 days to exclude any longer-term variations associated with the annual, seasonal, and intraseasonal variations to obtain the residual of the density. The density residuals from the five meteor radars are then employed to investigate the mesospheric density response to geomagnetic storms.

2.2. NOAA POES/MEPED Data

The Medium Energy Proton and Electron Detector (MEPED) in the package of Space Environment Monitor (SEM-2) instruments on board the NOAA Polar Orbiting Environmental Satellites (POES) includes a set of solid state energetic particle detectors that can monitor the intensities of protons and electrons over a range extending from 30 keV to more than 6,900 keV. In this study, the MEPED 0° proton detector is used to measure energetic proton precipitation (EPP) during solar proton events (SPEs). The P1–P6 differential energy proton channels of the MEPED are used for detection in the six different energy ranges of protons including 30–80; 80–240; 240–800; 800–2,500; 2,500–6,900; and >6,900 keV (see, e.g., Rodger et al., 2010; Ødegaard et al., 2016). Because the P6 channel may be contaminated by relativistic electrons (Yando et al., 2011), the proton measurements from this channel are disregarded. The proton flux measured by the P1–P5 energy channels is used to derive a world map distribution of EPP during geomagnetic storms.

3. Case Study

Figure 1 shows the world map distribution of EPP into the Earth's atmosphere during the geomagnetic storm on 17 March in 2015 (St. Patrick's Day). The St. Patrick's Day storm is the strongest geomagnetic storm of solar cycle 24 so far, with a *Dst* index minima of −223 nT. This storm was triggered by a coronal mass ejection (CME), accompanied by strong SPEs.

During SPEs, the EPP can be much stronger than the energetic electron precipitation (EEP) and can extend to lower latitudes (see, e.g., Andersson, Verronen, Rodger, Clilverd, & Wang, 2014). As shown in Figure 1, the EPP can reach 60°N in the European region (i.e., 0–90°E) and to near 40°N in the North American region (i.e., 60°W–120°W). In the Southern Hemisphere, the EPP can reach 45°S between 60°E and 150°E. The TMR is in the region of EPP, that is, the auroral zone; the SMR and the DMR are inside the auroral zone, noting however, that the EPP flux is relatively weaker than that for the TMR. The MMR is outside, but close to, the auroral zone during the storms. The BMR, located at midlatitudes, is outside and far from the auroral zone.

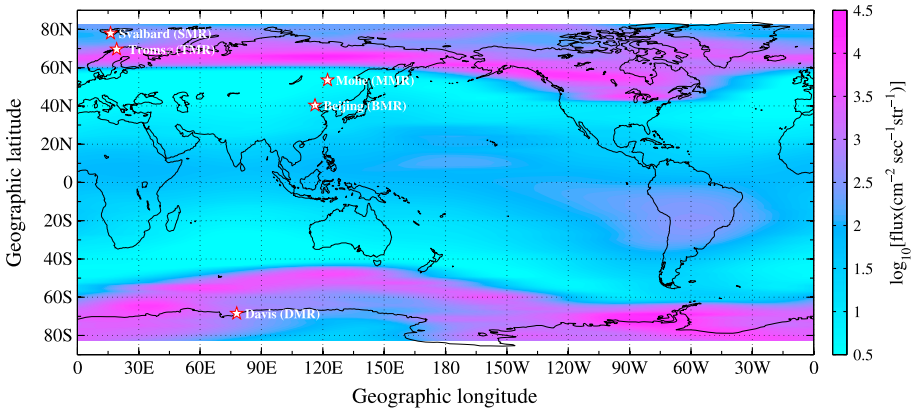

Figure 1. A world map showing the mean energetic proton precipitation observed by the 0° directed MEPED telescopes in geomagnetic storm on 17 March 2015. The stars represent the location of the meteor radars used in this study.

Figure 2 shows the mesospheric density response estimated from the five meteor radars to the two major geomagnetic storms. As shown in the left-hand column of Figure 2, the mesospheric density over the south (DMR) and north polar (SMR and TMR) show a very clear decrease during the St. Patrick's Day geomagnetic storm. The maxima of the density decrease observed by the DMR, SMR, and TMR reaches 23%, 14%, and 17%, respectively. The mesospheric density at higher midlatitudes observed by the MMR shows a slight decrease at 6%. The mesospheric density at lower midlatitudes from the BMR does not show a corresponding change during the storm.

As shown in the right-hand column of Figure 2, the southern polar mesospheric density from the DMR shows a sudden decrease on the day of the second geomagnetic storm. When compared to the southern polar mesospheric densities, the northern polar mesospheric densities seem to be more sensitive to this storm. Before the main phase of the 23 June 2015 (day 174) storm, there is a weak geomagnetic storm (minimum of $Dst = -51$ nT) on 22 June; however, the SMR, TMR, and MMR densities below 88 km all show obvious decreases (7%, 11%, and 5%, respectively) to this weak storm. During the main phase of the storm, the mesospheric density from the DMR, SMR, TMR, and MMR all show significant decreases, and the largest decrease (23%) in density is present in the TMR densities. In addition to these, there is another relatively weak storm on 25 June (day 176) during the recovery phase of the storm, and the DMR, SMR, TMR, and MMR densities also show a relatively weak decrease to this storm. We note that the observations indicate a synchronous change in mesospheric density in both the southern and northern polar regions driven by geomagnetic storms. We also note that dynamical influences from the lower atmosphere would not produce synchronous changes in each hemisphere. It is interesting to find that the BMR density seems also to be affected during the storms, with a 7% decreases to the storms on 23 and 25 June. However, the BMR density also shows a decrease before the storm, which suggests that the change in the BMR density is not solely in response to the intense storm, if at all.

The peak height of the meteor height distribution is an independent way of estimating the neutral mesospheric density and can serve as a proxy for the variation of the atmospheric density in the meteor ablation region (see, e.g., Stober et al., 2012; Yi, Reid, Xue, Younger, Spargo, et al., 2017; Yi, Reid, Xue, Younger, Murphy, et al., 2017). The absolute error of the peak height is less than 0.2 km. The peak height (black solid lines in Figure 2) estimated from the DMR, SMR, and TMR in polar region all show similar decreases with the mesospheric density during the two storms. This consistent variation of peak height with the mesospheric density estimated from the meteor radars during the storms can be used to exclude the possibility that the plasma of the ionospheric *D* region, chemical neutralization (see, e.g., Younger et al., 2014), and the geomagnetic field (see, e.g., Jones, 1991) are changed by the geomagnetic storms and are directly influencing the density values estimated from D_a.

It needs to be pointed out that apart from the influence of geomagnetic storms, the mesospheric density shown in the cases above may still be disturbed by the planetary wave propagated upward from below, and by planetary wave period variations generated by recurrent geomagnetic activity (Yi, Reid, Xue,

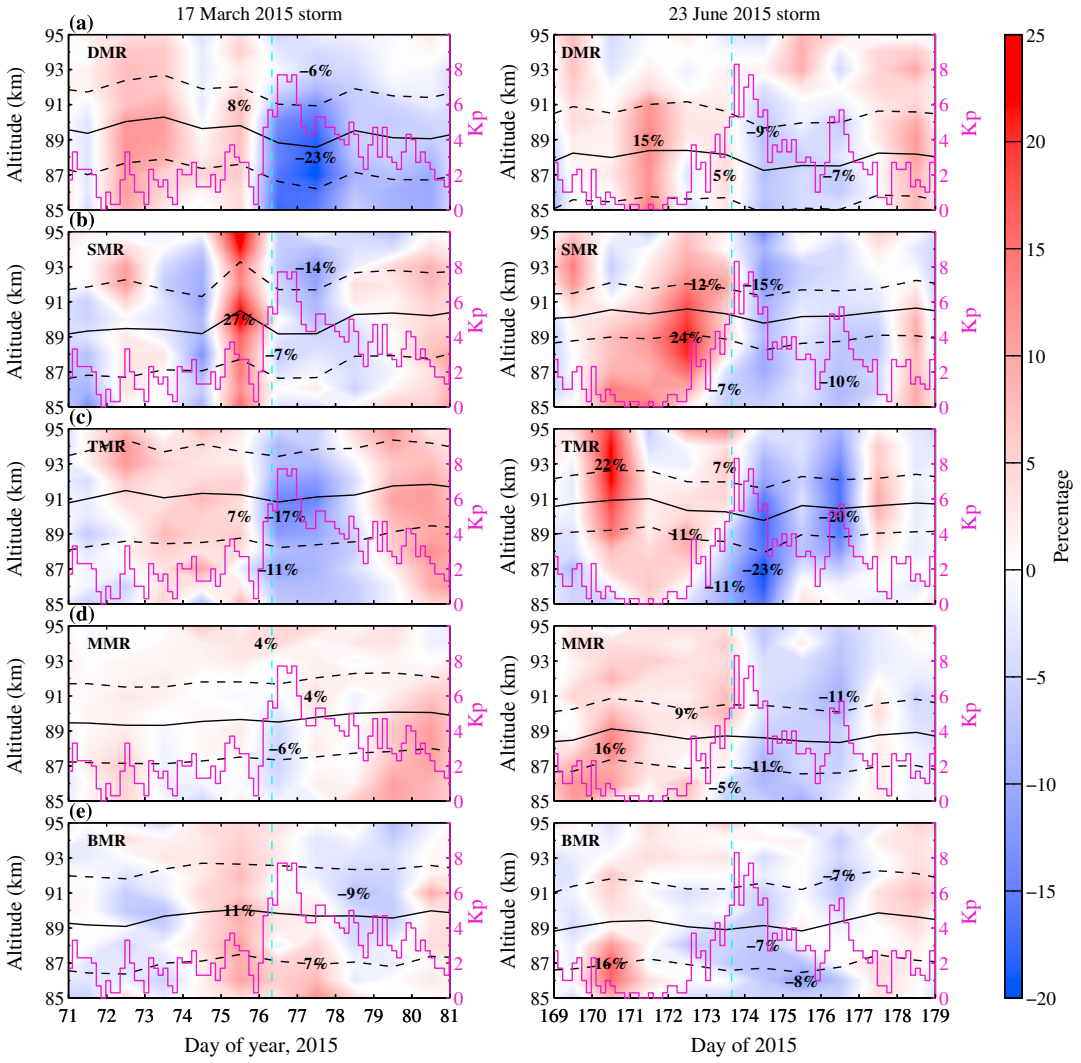

Figure 2. Daily neutral mesospheric density variations from 85 to 95 km estimated from (a) Davis Station, (b) Svalbard, (c) Tromsø, (d) Mohe, and (e) Beijing meteor radars during the geomagnetic storms on (left column) 17 March 2015 and on (right column) 23 June 2015. The color bar and black numbers indicate the percentage variations of the density residual to the mean density from ±7 days centered on the storm day. The black solid and dashed lines indicate the peak height and half-width (1/2 standard deviation) of the meteor height distribution. The purple line indicates the hourly *Kp* index, and the light blue dashed line indicates *Dst* less than −50 nT.

Younger, Spargo, et al., 2017; Yi, Reid, Xue, Younger, Murphy, et al., 2017). This is because we cannot effectively remove the effects of planetary wave period (2–20 days) variations in mesospheric density, because their characteristics are quite complex, with different wave patterns in different seasons and latitudes.

4. Statistical Results

To further examine the significance of geomagnetic storm effects on mesospheric density, we apply a statistical analysis. First, we select the super and intense geomagnetic storm candidates (minimum $Dst < -100$ nT) that fall within our meteor radar observation period from 2004.08 to 2016. If there is more than one storm event in 5 days, we select the first storm event and discard the other storm events in this 5 day period. Using these criteria, we select 29 geomagnetic storms (shown in Table S3 in the supporting information), including 2 super (minimum $Dst \leq -240$ nT) and 27 intense storms.

As shown in Figure 3, the mesospheric densities from the DMR, SMR, and TMR all show a decrease during the storms. During some events, the maximum decrease in the densities of the SMR and TMR reaches 20%. The

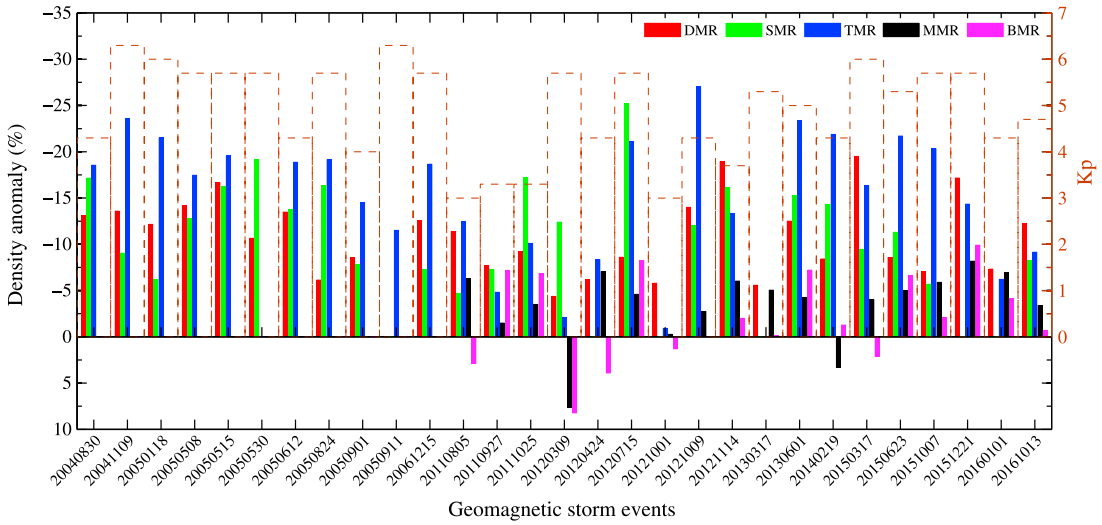

Figure 3. The relative change of the neutral mesospheric density at 90 km during selected geomagnetic storms. The percentage variations of the daily density residual on the storm day (that is, the day the *Dst* index reaches its minimum) with respect to the mean density from ±7 days centered on the geomagnetic storm day. The brown dashed bars indicate the values of daily *Kp* index of the geomagnetic storms.

90 km densities from the MMR show decreases during most of the events (16 of 18 events in total), especially those events occurring in the declining phase of solar cycle 24. The storm effects on the BMR density at 90 km are weaker than these at higher middle- and high-latitudes; for example, the BMR density shows a decrease during two thirds of the storm events (12 of 18 events in total). However, the amplitudes of the mesospheric density decrease do not seem to closely follow the strength of the geomagnetic storm as quantified by the value of the *Kp* index. Thus, it is likely in this case that the mesospheric density is influenced not only by the geomagnetic forcing from above but also by the effects of atmospheric waves such as planetary waves from below.

To examine the mesospheric density response to the geomagnetic storms quantitatively, we perform a superposed epoch analysis of data from the five meteor radars during the selected geomagnetic storms (shown in Table S3 in the supporting information). Superposed epoch analysis is useful when we have many observations of some event and are looking for responses to that event that are combined with noise from a lot of other influences. The polar region mesospheric densities estimated from the DMR, SMR, and TMR cover 28, 23, and 27 storm events, respectively. The observation times of the MMR and BMR (located at midlatitudes) are shorter than those for the polar region meteor radars. They do include 18 storm events, which is adequate for further statistical analysis to examine the midlatitude mesospheric density response to strong geomagnetic storms. The daily mesospheric density and peak height obtained from these five meteor radars, as well as the daily *Dst* and *AE* indices during the storm events are superposed on each other taking the day when the daily *Dst* indices reach the minima as the epoch day = 0 time.

Figures 4a–4c show that the superposed epoch mean mesospheric densities from the DMR, SMR, and TMR all have strong corresponding responses to the storm events. Before the storm (epoch day ≤ -2), the mesospheric densities under the auroral zone all show a clear increase, and the mean values of the densities increase more than 6%. During and after the storms (epoch day from -1 to 1), the mesospheric densities within the auroral zone all show significant decreases as the storms occur. The TMR density has the strongest decrease in response to the storms, with a 15% decrease on the day of storms (epoch day = 0). The SMR and DMR densities both have strong responses to the storms as well, with 12% and 11% decreases on the epoch day = 0, respectively. The peak heights obtained from the DMR, SMR, and TMR all show similar variations with the density response to the storms. The peak heights increase approximately 0.2 km before the storms, and then during the storms, the peak heights have strong decrease, with more than 0.4 km on the epoch day = 0. The superposed epoch mean values of *Dst* indices for the five data sets show a decrease beginning on the epoch day = -2 and reach the minima on epoch day = 0, and recover beginning on epoch day = 1. The *AE* indices show a clear anti-correlation with the density and peak height. The values of AE indices are low

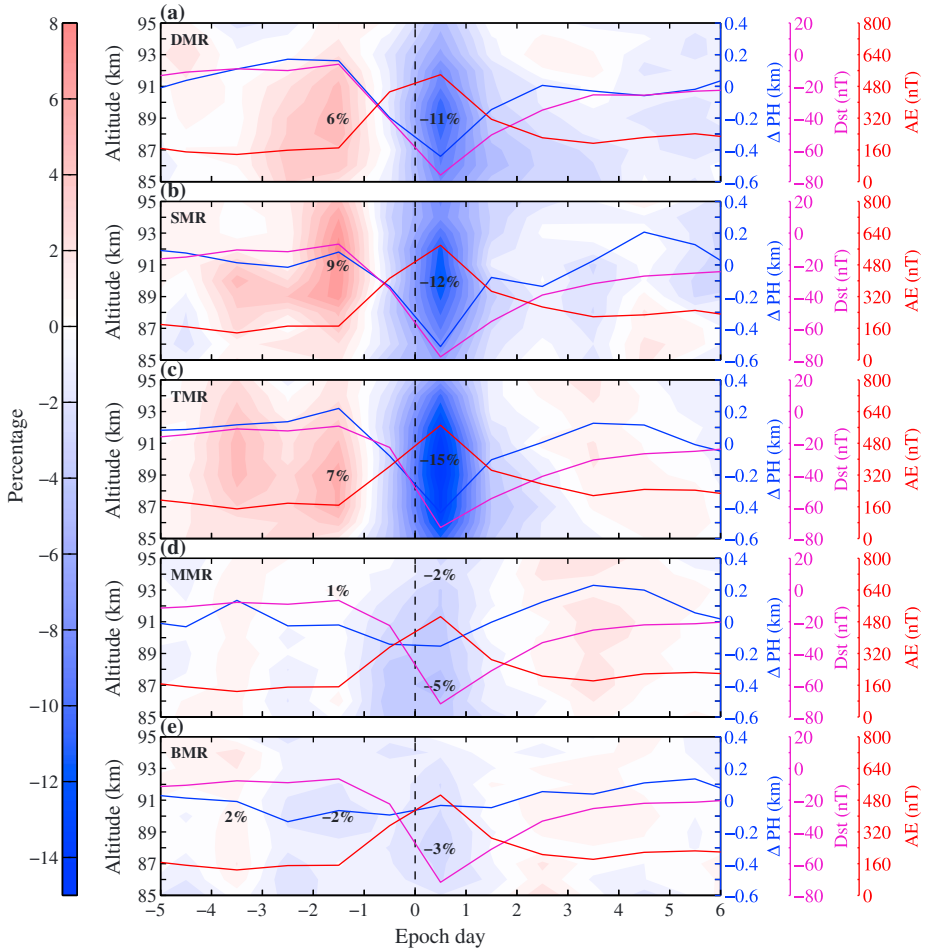

Figure 4. Contour plots of the results from superposed epoch analyses for the density estimated from (a) Davis Station (28 events), (b) Svalbard (23 events), (c) Tromsø (27 events), (d) Mohe (18 events), and (e) Beijing (18 events) meteor radars during the geomagnetic storms. The color bar and black numbers indicate the percentage variations of the density residual with respect to the mean density from ±7 days centered on the geomagnetic storm day. The blue lines indicate the mean values of the residual peak height during the geomagnetic storms, corresponding to the right blue axis. The purple and red lines indicate the mean values of the daily *Dst* and *AE* indices, during the geomagnetic storms, in each meteor radar observation time, corresponding to the right purple and red axes.

before the epoch day = −2, and after the epoch day = 2, and then increase and reach a maximum on the epoch day = 0 because of the strong energetic particle precipitation during storm periods.

The MMR density and peak height show a relatively weak decrease during the storms, with a 5% decrease of density below 91 km on epoch day = 0. The mesospheric density and peak height from the BMR (at a lower latitude) show the expected relatively weaker change during storm events. In order to confirm whether the mesospheric density changes obtained from MMR and BMR during the storms are truly affected by the storms, we carried out a similar superposed epoch analysis for 29 randomly selected events in each density residual, obtained from the five meteor radars. The random superposed epoch results in Figure S1 (supporting information) show that the variations of density from the five meteor radars are all quite small (<3%) and random; this is because the variation of the density residual is averaged out if we chose the events randomly. As shown in Figure S2 (supporting information), we also calculated the mean, median, 99%, and 90% confidence interval values by using 500 randomly superposed epochs from each meteor radar density and peak height residual data set. A similar approach has been described and applied by Andersson, Verronen, Rodger, Clilverd, and Seppälä (2014).

During superposed storm events, the average density and peak height decrease obtained from the DMR, SMR, and TMR are clearly larger than the 99% confidence levels (shown in Figure S2). The mean density

decrease obtained from the MMR below 91 km is larger than the 99% confidence level; above 91 km, the mean density decrease becomes smaller and lower than the 99% confidence level; however, it is still larger than the 90% confidence level. The mean peak height decrease obtained from the MMR is larger than the 90% confidence level. The average density and peak height decreases obtained from the BMR are basically lower than the 90% confidence level, which indicates that while the geomagnetic storm influences may extend to lower magnetic latitude regions, the effects are weaker and less significant. We also performed a similar superposed epoch analysis on the MLS mesospheric temperatures measured over the five meteor radars during the selected storms and found that the variations of MLS mesospheric temperature during the storms are small and random (as is shown in Figure S3 in the supporting information). The mesospheric temperature from the MLS does not seem to show a clear response to geomagnetic storms, the reason for which is still unclear.

5. Discussion and Summary

In sections 3 and 4 we have presented a case study and a statistical analysis, respectively, of the global mesospheric density response to geomagnetic storms. The mesospheric density near 90 km obtained from the meteor radars located under the auroral precipitation region shows a strong decrease associated with geomagnetic storms. Recently, Yi, Reid, Xue, Younger, Murphy, et al. (2017) reported a strong anticorrelation between the southern polar mesospheric density estimated from the DMR and recurrent geomagnetic activity driven by periodic corotating interaction regions (CIRs) in the declining phase of solar cycle 24 and that mesospheric density decreases as geomagnetic activity increases. They suggested as a possible mechanism that the mesospheric density decrease is due to mesospheric ozone depletion due to energetic particle precipitation, resulting in a loss of heating in the middle mesosphere (see, e.g., Andersson, Verronen, Rodger, Clilverd, & Seppälä, 2014; Daae et al., 2012, and references therein). Mesospheric dynamics, including zonal mean flow, the location of the polar vortex, and gravity wave propagation can be affected by a combination of Joule heating, chemical and radiative heating changes induced by geomagnetic activity (see review by Sinnhuber et al., 2012, and references therein; and, e.g., Hocke, 2017; Jackman et al., 2007; Yi, Reid, Xue, Younger, Murphy, et al., 2017). However, the actual mechanism of how MIT coupling during geomagnetic activity influences density at mesosphere heights is complex, and is still unclear for the moment.

In this study, we find that mesospheric density in the auroral region shows a significant decrease during geomagnetic storms. The response of mesospheric density is immediate, presenting a measureable response in less than 1 day (the best resolution of our meteor radar densities) of the onset of a geomagnetic storm. The statistical results show that the mesospheric density response of the TMR density is stronger than the DMR and SMR densities. This may be due to the TMR being located near the center of the auroral region and the area where EPP effects are most intense. In contrast, the DMR and SMR are located inside the auroral region, but at the edge of the region where EPP is significant (as shown in Figure 1).

In addition, we also found that the effect of strong geomagnetic storms on mesospheric density is not confined to the polar region but extends to higher midlatitudes sites like Mohe (outside the auroral region) most of the time. The influence of Joule and particle heating can penetrate down to mesosphere/lower-thermosphere (MLT) region heights and extend to midlatitudes during strong geomagnetic activity (e.g., Jiang et al., 2014; Sinnhuber et al., 2012). Yuan et al. (2015) reported a warming of the mesopause as observed by a midlatitude lidar in North America (geomagnetic latitude, 49°N) during strong geomagnetic storms induced by CMEs, and suggested that the warming was most likely due to equatorward transport from the Joule and particle heated region at high latitudes. Referring to these studies, we can speculate that the impact of strong geomagnetic storms could affect the global circulation in the MLT region and then influence the mesospheric density outside the auroral region. This would be consistent with the MMR density in midlatitude showing a relatively weak, but still measurable, decrease in response to geomagnetic storms.

Finally, we examined the polar mesospheric density derived from the NRLMSISE-00 (Picone et al., 2002) and the Whole Atmosphere Community Climate Model with thermosphere and ionosphere extension (WACCM-X) (Liu et al., 2010) in response to geomagnetic activity. The NRLMSISE-00 density shows a decrease in the lower thermosphere and an increase in the mesosphere as the geomagnetic activity enhances. The mesospheric density in WACCM-X shows no obvious response to geomagnetic activity. The differences

between the models, and the observations and the models, suggest that physical and chemical processes in the mesosphere during geomagnetic activity are not presently incompletely captured. This is the subject of ongoing work.

This is the first time interhemisphere observations of a neutral mesospheric density response to geomagnetic storms have been reported and reveals a direct coupling between the Sun and the Earth's mesosphere through an interaction between the solar wind and the Earth's MIT system. Considering the more than ~10% decrease in polar mesospheric density during storms, it is reasonable to expect that geomagnetic storms influence the mesospheric dynamics. This raises a challenge to modeling work aimed at understanding the possible physics and chemical connection in the mesosphere and MIT coupling during geomagnetic storms.

Acknowledgments

This work is supported by the National Natural Science Foundation of China (41774158, 41474129, and 41674150), the Chinese Meridian Project, the Youth Innovation Promotion Association of the Chinese Academy of Sciences (2011324), and the China Scholarship Council. We also acknowledge support provided by the University of Adelaide and ATRAD Pty Ltd, and the provision of Davis meteor radar data by the Australian Antarctic Division, the provision of Nippon/Norway Svalbard and Tromsø meteor radar data by the National Institute of Polar Research and UiT-The Arctic University of Norway, the provision of Mohe and Beijing meteor radar data by the Chinese Meridian Project and STERN (the Solar: Terrestrial Environment Research Network). Operation of the Davis meteor radar was supported under AAS project 2529, 2668, and 4025. Davis meteor radar data are available from the Australian Antarctic Data Centre at data.aad.gov.au. We thank the NASA EOS Aura MLS team and the NOAA POES/SEM-2 team for providing free access to their data. Aura/MLS data are available from http://disc.sci.gsfc.nasa.gov/Aura/data-holdings/MLS. The POSE/SEM-2/MEPED data are available from https://www.ngdc.noaa.gov/stp/satellite/poes/index.html. The *Kp*, *Dst*, *Ap*, and $F_{10.7}$ data were obtained from the Goddard Space Flight Centre / Space Physics Data Facility (GSFC/SPDF) OMNIWeb interface (https://omniweb.gsfc.nasa.gov/ow.html).

References

Andersson, M. E., Verronen, P. T., Rodger, C. J., Clilverd, M. A., & Seppälä, A. (2014). Missing driver in the Sun–Earth connection from energetic electron precipitation impacts mesospheric ozone. *Nature Communications*, *5*, 5197. https://doi.org/10.1038/ncomms6197

Andersson, M. E., Verronen, P. T., Rodger, C. J., Clilverd, M. A., & Wang, S. (2014). Longitudinal hotspots in the mesospheric OH variations due to energetic electron precipitation. *Atmospheric Chemistry and Physics*, *14*(2), 1095–1105. https://doi.org/10.5194/acp-14-1095-2014

Daae, M., Espy, P., Nesse Tyssøy, H., Newnham, D., Stadsnes, J., & Søraas, F. (2012). The effect of energetic electron precipitation on middle mesospheric night-time ozone during and after a moderate geomagnetic storm. *Geophysical Research Letters*, *39*, L21811. https://doi.org/10.21029/22012GL053787

Forbes, J. M., & Garrett, H. B. (1979). Theoretical studies of atmospheric tides. *Reviews of Geophysics and Space Physics*, *17*(8), 1951–1981. https://doi.org/10.1029/RG017i008p01951

Fritts, D. C., & Alexander, M. J. (2003). Gravity wave dynamics and effects in the middle atmosphere. *Reviews of Geophysics*, *41*(1), 1003. https://doi.org/10.1029/2001RG000106

Gao, H., Xu, J., Smith, A. K., & Chen, G.-M. (2017). Effects of solar proton events on dayglow observed by the TIMED/SABER satellite. *Journal of Geophysical Research: Space Physics*, *122*, 7619–7635. https://doi.org/10.1002/2017JA023966

Hall, C. M., Aso, T., Tsutsumi, M., Höffner, J., Sigernes, F., & Holdsworth, D. A. (2006). Neutral air temperatures at 90 km and 70°N and 78°N. *Journal of Geophysical Research*, *111*, D14105. https://doi.org/10.1029/2005JD006794

Hocke, K. (2017). Response of the middle atmosphere to the geomagnetic storm of November 2004. *Journal of Atmospheric and Solar: Terrestrial Physics*, *154*, 86–91. https://doi.org/10.1016/j.jastp.2016.12.013

Holdsworth, D. A., Reid, I. M., & Cervera, M. A. (2004). Buckland Park all-sky interferometric meteor radar. *Radio Science*, *39*, RS5009. https://doi.org/10.1029/2003RS003014

Jackman, C. H., DeLand, M. T., Labow, G. J., Fleming, E. L., Weisenstein, D. K., Ko, M. K. W., … Russell, J. M. (2005). Neutral atmospheric influences of the solar proton events in October–November 2003. *Journal of Geophysical Research*, *110*, A09S27. https://doi.org/10.1029/2004JA010888

Jackman, C. H., Roble, R. G., & Fleming, E. L. (2007). Mesospheric dynamical changes induced by the solar proton events in October–November 2003. *Geophysical Research Letters*, *34*, L04812. https://doi.org/10.1029/2006GL028328

Jiang, G., Wang, W., Xu, J., Yue, J., Burns, A. G., Lei, J., & Rusell, J. M. III (2014). Responses of the lower thermospheric temperature to the 9 day and 13.5 day oscillations of recurrent geomagnetic activity. *Journal of Geophysical Research*, *119*, 4841–4859. https://doi.org/10.1002/2013JA019406

Jones, W. (1991). Theory of diffusion of meteor trains in the geomagnetic field. *Planetary and Space Science*, *39*(9), 1283–1288. https://doi.org/10.1016/0032-0633(91)90042-9

Liu, H.-L., Foster, B. T., Hagan, M. E., McInerney, J. M., Maute, A., Qian, L., … Oberheide, J. (2010). Thermosphere extension of the whole atmosphere community climate model. *Journal of Geophysical Research*, *115*, A12302. https://doi.org/10.1029/2010JA015586

Liu, L., Liu, H., Chen, Y., Le, H., Sun, Y.-Y., Ning, B., … Wan, W. (2016). Variations of the meteor echo heights at Beijing and Mohe, China. *Journal of Geophysical Research: Space Physics*, *121*, 1117–1127. https://doi.org/10.1002/2016JA023448

Ødegaard, L.-K. G., Tyssøy, H. N., Sandanger, M. I. J., Stadsnes, J., & Søraas, F. (2016). Space weather impact on the degradation of NOAA POES MEPED proton detectors. *Journal of Space Weather and Space Climate*, *6*, A26. https://doi.org/10.1051/swsc/2016020

Picone, J. M., Hedin, A. E., Drob, D. P., & Aikin, A. C. (2002). NRLMSISE-00 empirical model of the atmosphere: Statistical comparisons and scientific issues. *Journal of Geophysical Research*, *107*(A12), 1468. https://doi.org/10.1029/2002JA009430

Rodger, C. J., Clilverd, M. A., Green, J. C., & Lam, M. M. (2010). Use of POES SEM-2 observations to examine radiation belt dynamics and energetic electron precipitation into the atmosphere. *Journal of Geophysical Research*, *115*, A04202. https://doi.org/10.1029/2008JA014023

Salby, M. L. (1984). Survey of planetary-scale traveling waves: The state of theory and observations. *Reviews of Geophysics*, *22*, 209–236. https://doi.org/10.1029/RG022i002p00209

Schwartz, M. J., Lambert, A., Manney, G. L., Read, W. G., & Livesey, N. J. (2008). Validation of the Aura Microwave Limb Sounder temperature and geopotential height measurements. *Journal of Geophysical Research*, *113*, D15S11. https://doi.org/10.1029/2007JD008783

Sinnhuber, M., Nieder, H., & Wieters, N. (2012). Energetic particle precipitation and the chemistry of the mesosphere/lower thermosphere. *Surveys in Geophysics*, *33*(6), 1281–1334. https://doi.org/10.1007/s10712-012-9201-3

Solomon, S., Rusch, D. W., Thomas, R. J., & Eckman, R. S. (1983). Comparison of mesospheric ozone abundance measured by the solar mesosphere explorer and model calculations. *Geophysical Research Letters*, *10*, 249–252. https://doi.org/10.1029/GL010i004p00249

Stober, G., Jacobi, C., Matthias, V., Hoffmann, P., & Gerding, M. (2012). Neutral air density variations during strong planetary wave activity in the mesopause region derived from meteor radar observations. *Journal of Atmospheric and Solar - Terrestrial Physics*, *74*, 55–63. https://doi.org/10.1016/j.jastp.2011.10.007

Takahashi, H., Nakamura, T., Tsuda, T., Buriti, R. A., & Gobbi, D. (2002). First measurement of atmospheric density and pressure by meteor diffusion coefficient and airglow OH temperature in the mesopause region. *Geophysical Research Letters*, *29*(8), 1165. https://doi.org/10.1029/2001GL014101

von Savigny, C., Sinnhuber, M., Bovensmann, H., Burrows, J. P., Kallenrode, M.-B., & Schwartz, M. (2007). On the disappearance of noctilucent clouds during the January 2005 solar proton events. *Geophysical Research Letters*, *34*, L02805. https://doi.org/10.1029/2006GL028106

Yando, K., Millan, R. M., Green, J. C., & Evans, D. S. (2011). A Monte Carlo simulation of the NOAA POES medium energy proton and electron detector instrument. *Journal of Geophysical Research*, *116*, A10231. https://doi.org/10.1029/2011JA016671

Yi, W., Reid, I. M., Xue, X., Younger, J. P., Murphy, D. J., Chen, T., & Dou, X. (2017). Response of neutral mesospheric density to geomagnetic forcing. *Geophysical Research Letters*, *44*, 8647–8655. https://doi.org/10.1002/2017GL074813

Yi, W., Reid, I. M., Xue, X., Younger, J. P., Spargo, A. J., Murphy, D. J., … Dou, X. (2017). First observation of mesosphere response to the solar wind high-speed streams. *Journal of Geophysical Research: Space Physics*, *122*, 9080–9088. https://doi.org/10.1002/2017JA024446

Younger, J. P., Lee, C. S., Reid, I. M., Vincent, R. A., Kim, Y. H., & Murphy, D. J. (2014). The effects of deionization processes on meteor radar diffusion coefficients below 90 km. *Journal of Geophysical Research*, *119*, 10,027–10,043. https://doi.org/10.1002/2014JD0217

Yuan, T., Zhang, Y., Cai, X., She, C.-Y., & Paxton, L. J. (2015). Impacts of CME induced geomagnetic storms on the midlatitude mesosphere and lower thermosphere observed by a sodium lidar and TIMED/GUVI. *Geophysical Research Letters*, *42*, 7295–7302. https://doi.org/10.1002/2015GL064860